A MALDI-TOF assay identifies nilotinib as an inhibitor of inflammation in acute myeloid leukemia and multiple myeloma.

Rachel E. Heap[1,#], José Luis Marín-Rubio[1,#,*], Tiaan Heunis[1,2], Maria Emilia Dueñas[1], Joseph Inns[1], Barbara Saxty[3] and Matthias Trost[1,*].

[1] Laboratory for Biological Mass Spectrometry, Biosciences Institute, Newcastle University, Newcastle-upon-Tyne, NE2 4HH, UK

[2]Sir William Dunn School of Pathology, University of Oxford, South Parks Road, Oxford OX1 3RE, UK

[3] LifeArc, SBC Open Innovation Campus, Stevenage, SG1 2FX, UK

[#]These authors contributed equally to this work.

* Corresponding author:

Matthias Trost, Tel: +44 191 2087009, E-mail: matthias.trost@ncl.ac.uk

José Luis Marín-Rubio, Tel +44 191 2088983 E-mail: jose.marin-rubio@newcastle.ac.uk

Key Points

Label-free cell-based assay identifies new anti-inflammatory drugs using MALDI-TOF MS.

Nilotinib reduces inflammation by inhibition of MAPK14 in AML and MM.

Topics: MALDI-TOF, nilotinib, inflammation, myeloma, leukemia, high-throughput drug discovery

ABSTRACT

Inflammatory responses are important in cancer, particularly in the context of monocyte-rich aggressive myeloid neoplasm. We developed a label-free cellular phenotypic drug discovery assay to identify anti-inflammatory drugs in human monocytes derived from acute myeloid leukemia (AML), by tracking several biological features ionizing from only 2,500 cells using matrix-assisted laser desorption/ionization-time of flight (MALDI-TOF) mass spectrometry. A proof-of-concept screen showed that the BCR-ABL inhibitor nilotinib, but not the structurally similar imatinib, blocks inflammatory responses. In order to identify the cellular (off-)targets of nilotinib, we performed thermal proteome profiling (TPP) using TMTpro 16plex. Unlike imatinib, nilotinib inhibits p38-alpha (MAPK14) signalling. This inhibition suppressed the expression of inflammatory cytokines, cell adhesion and innate immunity markers in activated human monocytes derived from AML. Thus, our study provides a tool for the discovery of new anti-inflammatory drugs, which could contribute to the treatment of inflammation in myeloid neoplasms and other diseases.

INTRODUCTION

Monocyte-derived macrophages play important roles in both physiological and pathological processes. The activation of these cells during pathogen infection or other insults leads, in part, to the pathophysiology of inflammation.[1] Monocytes can recognize various damage-associated molecular (DAMPs) and pathogen-associated molecular patterns (PAMPs) through specific receptors, such as Toll-like receptors (TLRs). Activation of these receptors leads to the production of cytokines, chemokines, and mediators that are involved in inflammation in myeloid leukemia.[2,3] Several hematopoietic disorders, including lymphoproliferative disorders and myelodysplastic syndromes, which possess a high risk of transformation to leukemia, have been linked to aberrant TLR signalling.[4,5] Moreover, TLR2 and TLR4 show significantly higher expression in the bone marrow of patients with myeloid leukemia.[5] While TLRs are specific for exogenous PAMPs such as lipopolysaccharide (LPS) which triggers TLR4 signalling in monocytes and macrophages, they are also activated by specific endogenous DAMPs such as HSP60 or biglycan.[6,7] TLR activation leads to intracellular signalling cascades including the mitogen-activated kinase (MAP) pathways,[8,9] increasing the expression and secretion of inflammatory cytokines and chemokines including interleukins (IL-6, IL-8 and IL-10), interferons (IFN), and tumor necrosis factor alpha (TNF-α).[10]

The discovery of drugs that prevent chronic or acute inflammation is a major goal of the pharmaceutical industry for the treatment of infectious diseases, autoimmune diseases, and cancer.[11] The discovery and design of new compounds for inhibiting inflammation are typically achieved through high-throughput screening (HTS) approaches, however, fluorescence and chemiluminescence methodologies cannot be used in primary cells and

other read-outs, including antibody-based assays such as ELISA, are very expensive.[12,13] As such, there is a growing need to develop physiological phenotypic HTS assays that can be used in monocytic cells to accelerate the discovery of inhibitors.[14,10z5] Matrix-assisted laser desorption/ionization-time of flight (MALDI-TOF) mass spectrometry (MS) is a versatile, label-free technique that has the potential to accelerate HTS of promising drug candidates.[16-18] In this study, we developed a MALDI-TOF MS cellular assay to perform a blind screen of 96 compounds to assess their potential anti-inflammatory effects on human monocytes derived from acute myeloid leukemia (AML). We discovered that nilotinib, but not the structurally related imatinib, inhibits inflammatory signalling. Using Thermal Proteome Profiling (TPP), we can show that nilotinib blocks the p38α MAP kinase pathway. Overall, our data show that nilotinib is a drug capable of preventing inflammation in AML and multiple myeloma (MM).

RESULTS

A novel MALDI-TOF MS cellular assay to characterize inflammatory phenotypes

Recently, high-throughput MALDI-TOF MS has been used successfully for *in vitro* assays of specific enzymes. Here, we tested if MALDI-TOF MS can be used for phenotypic assays to monitor inflammatory responses by identifying differences in the "fingerprint" of biomolecules ionized when whole cells are spotted onto the MALDI target (**Figure 1A**). As a proof of concept, we tested if we could distinguish phenotypes of THP-1 cells, a model of human monocytes derived from AML,[19] upon stimulation with a number of pro-inflammatory stimuli, namely LPS, Pam2CSK4, Pam3CSK4; which activate TLR4, TLR1/2 and TLR2/6, respectively, as well as interferon-γ (IFN-γ). Principal component analysis (PCA) of all biomolecules detected in the range of *m/z* 2,000-20,000 showed clear separation of monocytes treated with TLR-agonists, while IFN-γ treatment did not separate from untreated, suggesting that the features are not interferon-stimulation dependent but rather TLR dependent (**Figure 1B**). A loading plot analysis of the PCA results identified the two features at *m/z* 4632 and 4964 as the main drivers for the difference in the phenotypes (**Figure 1C**). The feature *m/z* 4632 was significantly reduced while *m/z* 4964 increased in LPS-stimulated cells (**Figure 1D-E**). We confirmed that other TLR ligands such as Pam2CSK4 and Pam3CSK4, which activate TLR1/2 and TLR2/6, respectively, did also increase this ratio and in a dose-dependent manner, while interferon-gamma (IFN-γ) did not affect it (**Figure 1F-G**). Thus, we used the feature at *m/z* 4632 as a resting phenotype biomarker and feature *m/z* 4964 as an LPS-stimulated monocyte phenotype biomarker. To verify that this phenotype was not due to cell death, we treated the cells with 0.5 µM staurosporine for 24h before analysis with our MALDI-TOF assay. Our results showed that apoptosis leads to a distinct cluster in the PCA compared to control or LPS-treated cells (**Figure 1H**), suggesting

that this assay can be multiplexed to identify other phenotypes such as cell toxicity. Together, these results indicate that biomarkers identified by MALDI-TOF MS can be used to detect changes in the inflammatory phenotype downstream of TLRs in AML cells.

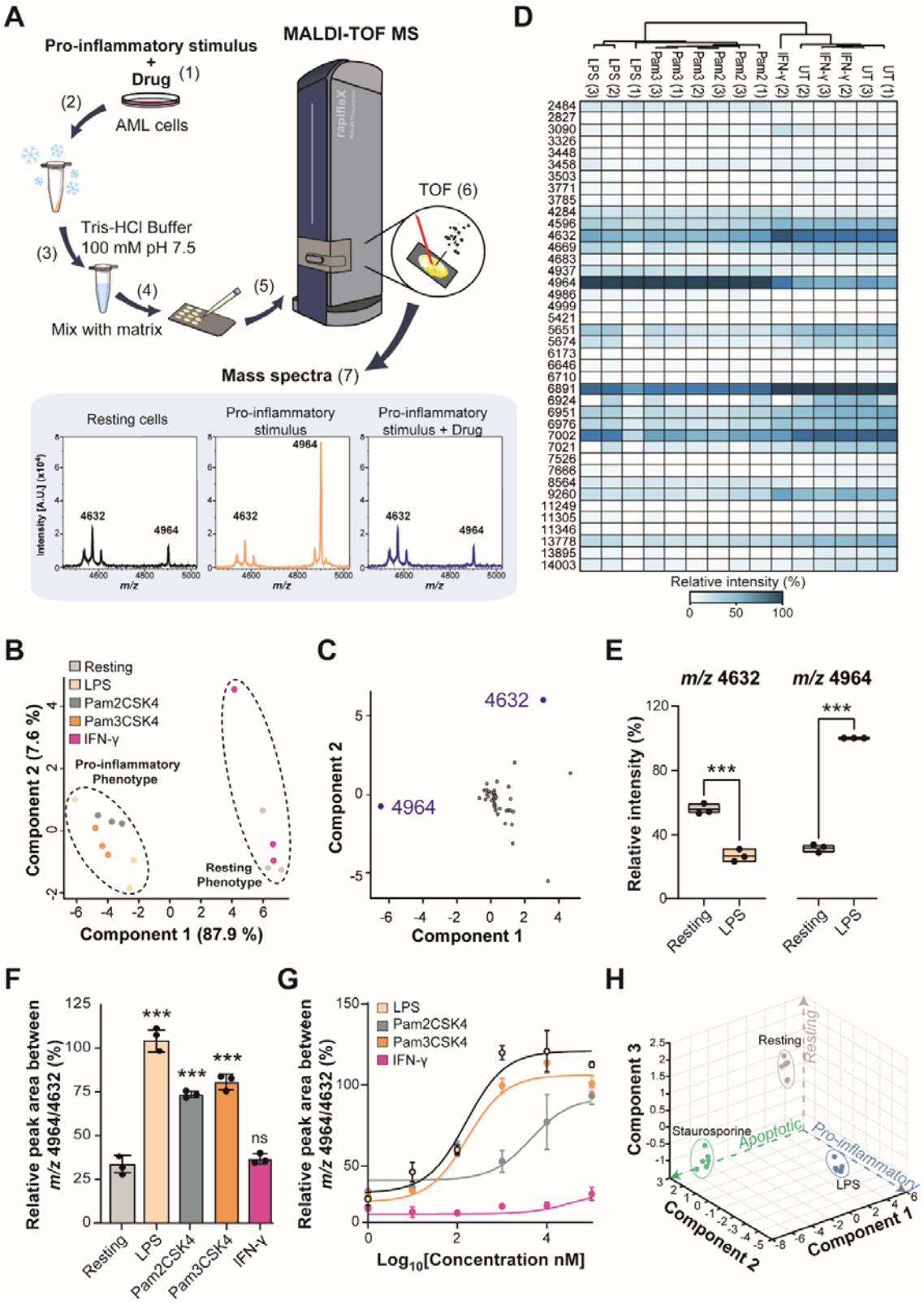
A
Pro-inflammatory stimulus
+
Drug (1)
(2)
AML cells
Tris-HCl Buffer
100 mM pH 7.5
(3)
(4)
Mix with matrix
(5)
MALDI-TOF MS
TOF (6)
Mass spectra (7)
Resting cells
Pro-inflammatory stimulus
Pro-inflammatory stimulus + Drug
4632
4964
Intensity [A.U.] (x10⁴)
m/z
D
Relative intensity (%)
0
50
100
B
Resting
LPS
Pam2CSK4
Pam3CSK4
IFN-γ
Pro-inflammatory Phenotype
Resting Phenotype
Component 2 (7.6 %)
Component 1 (87.9 %)
C
4632
4964
Component 2
Component 1
E
m/z 4632
m/z 4964
Relative intensity (%)
***
Resting
LPS
F
Relative peak area between m/z 4964/4632 (%)
***
ns
Resting
LPS
Pam2CSK4
Pam3CSK4
IFN-γ
G
LPS
Pam2CSK4
Pam3CSK4
IFN-γ
Relative peak area between m/z 4964/4632 (%)
Log10[Concentration nM]
H
Resting
Staurosporine
Apoptotic
Pro-inflammatory
LPS
Component 3
Component 2
Component 1

101

102 **Figure 1. Identification of features associated with the monocyte inflammatory phenotype by**
103 **MALDI-TOF MS. A)** Workflow of the MALDI-TOF MS assay: (1) AML cells were pre-treated with a
104 drug for 1h before adding a pro-inflammatory stimulus for 24h. (2) Cells were frozen on dry ice,
105 thawed and (3) washed with 100 mM Tris-HCl buffer at 4°C. (4) Cells were mixed with a matrix (10
106 mg/mL α-cyano-4-cinnamic acid in 50% acetonitrile, 0.1% trifluoroacetic acid). (5) Cells were
107 analysed in a RapifleX PharmaPulse MALDI TOF mass spectrometer. (6 In the ionization chamber a
108 laser is used to produce ions in the gas phase. These ions are separated according to their time-of-
109 free flight (TOF: Time-Of-Flight). The smaller molecules reach the detector first, followed by the
110 bigger, according to the *m/z* ratio. (7) The detector converts the received ions into electrical current
111 which is amplified and digitized in the m/z spectra. **B)** Unsupervised PCA plot of LPS, Pam2CSK4,
112 Pam3CSK4 and IFN-γ-treated cells showing separation of cells treated with bacterial ligands treated
113 and resting monocytes. **C)** Loading plot derived from PCA in B) showing that m/z 4964 and 4632
114 contribute predominantly to the separation of the two clusters in component 1 and component 2. **D)**
115 Unsupervised heat map of the relative intensities of three biological replicates of THP-1 cells treated
116 with 100 ng/mL LPS, Pam2CSK3, Pam2CSK4 and 100 U/mL IFN-γ for 24h compared with resting cells
117 **E)** Box plots of significantly changing intensities between resting and LPS-treated monocytes
118 identified at *m/z* 4632 and 4964. **F)** Relative quantitation from three biological replicates of THP-1
119 cells treated with 100 ng/mL LPS, Pam2CSK3, Pam2CSK4 and 100 U/mL IFN-γ for 24h compared with
120 resting cells. **G)** Titration of LPS, Pam2CSK4 and Pam3CSK4-treated cells from 10 - 100 ng/mL of
121 stimulus. **H)** PCA plot with three dimensions represents resting, LPS-, and 0.5 μM staurosporine-
122 treated cells. Significant differences between two groups were determined by a Students t-test. The
123 statistical significance of the comparisons with resting is indicated as follows: ns, not significant;
124 ***, $P \leq 0.001$. Error bars represent the SEM.
125

126 **The MALDI-TOF MS cellular assay can detect inhibitors of inflammation**

127 Next, we used the TAK1 inhibitor NG-25, which blocks TNF-α production, the TBK1 inhibitor
128 MRT67303, which blocks production of type I interferons (IFNs),[20,21] as well as BI2536, a
129 PLK1 inhibitor that has been show to inhibit pro-inflammatory gene transcription due to
130 inhibition of BET proteins[22], to test if pharmacological inhibition of these pathways can be
131 detected in our assay (**Figure 2A**). THP-1 cells were pre-treated with the inhibitors for one
132 hour before LPS-stimulation. NG-25 and BI2536 treatment, but not MRT67303, reduced
133 TNF-α secretion (**Figure 2B)**. Comparably, our MALDI-TOF MS assay showed that treatment
134 with NG-25 or BI2536 blocked the inflammatory phenotype and was indistinguishable to
135 vehicle control cells not treated with LPS, while MRT67307-treated cells still showed an
136 increased ratio at *m/z* 4964/4632, similar to LPS-treated cells (**Figure 2C**). Moreover, using
137 all biomolecule features, PCA analysis showed that treatment with NG-25 and BI2536
138 reverted the features back close to control, while MRT67307 did not affect LPS-induced
139 features significantly (**Figure 2D**). This data shows that pharmacological intervention of
140 inflammatory pathways can be detected by our assay and that NG-25 and MRT67307 can be
141 used as positive and negative control compounds in high-throughput screens, respectively.
142

143 **Label-free MALDI-TOF MS identifies nilotinib as an anti-inflammatory compound**

144 Once the analytical workflow was established to identify an inflammatory phenotype in
145 THP1 cells, we evaluated the potential of the assay to discriminate positive and negative
146 inhibitors of inflammation in a proof-of-concept blind screen of 96 selected kinase inhibitors
147 (**Supplementary Table 1).** The assay showed very good sensitivity (z'=~0.8) and
148 reproducibility ($R^2 > 0.8$**) (Supplementary Figure 1A-B**). Only two positive hits were observed
149 when applying a cut-off of 40% to the ratio *m/z* 4964/4632. Unblinding revealed that these
150 compounds were NG-25 and nilotinib (Tasigna®) (**Figure 2E)**. Nilotinib is a BCR-ABL tyrosine

151 kinase inhibitor[23,24] and is a second-generation derivative of imatinib (Gleevec®),[24] which
152 was also included in the panel screened. However, imatinib did not affect the phenotype of
153 inflammatory monocytes, while nilotinib-treated monocytes did not display an LPS-induced
154 inflammatory phenotype and showed no differences compared to non-activated monocytes
155 in the ratio of *m/z* 4964/4632 (**Figure 2F**).
156 In order to validate the MALDI-TOF MS results, we measured secreted TNF-α levels in THP-1
157 cells treated with each inhibitor. Nilotinib treatment reduced expression and secretion
158 levels of TNF-α, while imatinib did not affect TNF-α levels upon LPS treatment (**Figure 2G-H**).
159 Both MALDI-TOF MS and TNF-α ELISA data provided a similar IC50 of approximately 400-500
160 nM for the inhibitory effect of Nilotinib (**Supplementary Figure 1C-D**). This data indicates
161 that nilotinib is able to block inflammatory responses downstream of TLR activation, while
162 the structurally similar imatinib cannot.
163

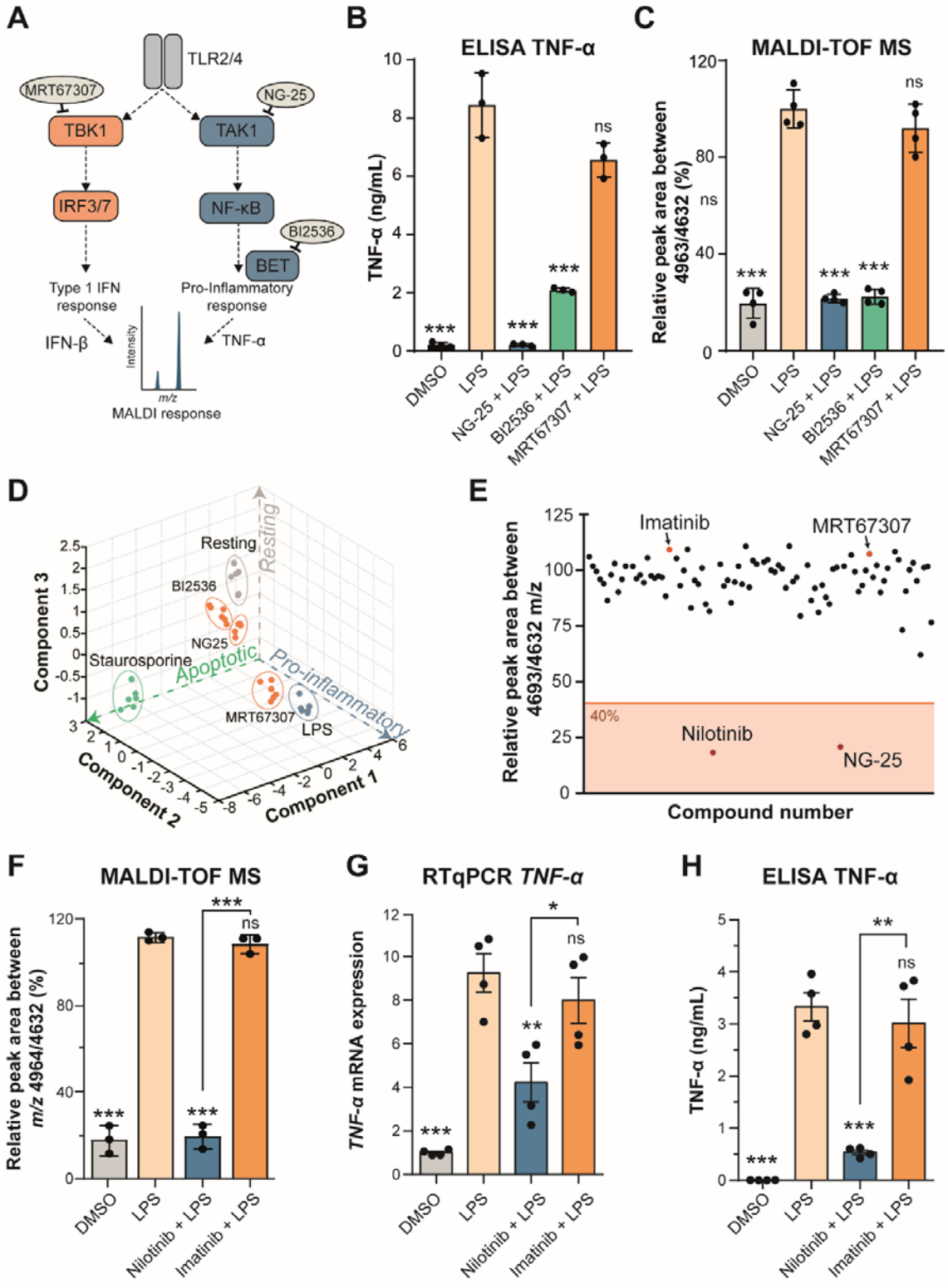

Figure 2. Nilotinib is a positive hit in a cellular MALDI-TOF MS drug discovery screen and inhibits inflammation in response to LPS. A) Inhibition of the TLR2 and TLR4 signalling pathways. MRT67307

167 inhibits TBK1 (TANK Binding Kinase 1) which blocks production of type I interferons (IFNs). NG-25
168 inhibits TAK1 (TGF-Beta-Activated Kinase 1) which induces TNF-α and IL-6 production. BI2536 inhibits
169 BET proteins (Bromodomain and Extra-Terminal motif proteins) which are required for pro-
170 inflammatory gene transcription. **B)** TNF-α secretion of THP-1 cells treated in either vehicle control-
171 treated (DMSO), 100 ng/mL LPS-treated, or pre-treated with 5 µM NG-25, BI2536 or MRT67307 for
172 one hour before 100 ng/mL LPS-treatment for up to 24h measured by ELISA. **C)** MALDI-TOF MS
173 relative quantitation of the ratio *m/z* 4964/4632 in THP-1 cells as treated in B). **D)** PCA of all features
174 identified by the MALDI-TOF MS of experiment in B). **E)** Compound hit map of the mean of three
175 biological replicates with 40% effectiveness cut off showing nilotinib and NG-25 as positive hits and
176 imatinib and MRT67307 as negative hits (arrows). **F)** MALDI-TOF MS relative quantitation of the ratio
177 *m/z* 4964/4632 in THP-1 cells in vehicle control-treated (DMSO), 100 ng/mL LPS-treated, or pre-
178 treated with 5 µM nilotinib or imatinib for one hour before 100 ng/mL LPS-treatment for up to 24h.
179 **G)** *TNF-α* expression of cells treated as in F.) determined by RT-qPCR at 24 h. The results were
180 analysed using the $2^{-\Delta\Delta Ct}$ method and normalized using *GAPDH* and *TBP* as the reference genes and
181 vehicle control (DMSO) as the reference sample. Significant differences between two groups were
182 determined by a Students t-test. **H)** TNF-α secretion of cells treated as in F.) measured by ELISA after
183 24h. The statistical significance of the comparisons with LPS is indicated as follows: ns, not
184 significant; *, $P \leq 0.05$; **, $P \leq 0.01$; ***, $P \leq 0.001$. Error bars represent the SEM of three (**B**, **F**) or
185 four (**C**, **G, H**) biological replicates.
186

187 **Nilotinib blocks the inflammatory response by inhibiting the p38α MAP kinase pathway.**

188 Nilotinib is known to inhibit BCR-ABL and other tyrosine kinases.[24] A putative role of these
189 kinases in inflammatory signalling downstream of TLRs is unknown. Moreover, the kinase
190 potentially involved in this particular function must be a specific nilotinib target, since the
191 treatment with imatinib did not result in the same phenotype. In order to identify the off-

192 targets responsible for the nilotinib-specific anti-inflammatory phenotype, we performed
193 thermal proteome profiling (TPP) by multiplexed quantitative mass spectrometry using
194 tandem mass tags (TMT) (**Figure 3A**, **Supplementary Table 2, and Supplementary Table 3)**.
195 This method is based on determining the changes in the thermal stability of proteins, which
196 may be due to direct drug binding, drug-induced conformation changes, binding to other
197 cellular components, or post-translational modifications such as phosphorylation.[25-29] We
198 pre-treated THP1 cells for 1 h with nilotinib or imatinib before stimulation with LPS for 15
199 min. We reduced the LPS treatment to 15 min in order to avoid changes in protein
200 abundance due to transcriptional responses to LPS activation. Overall, we identified 5,565
201 proteins in our TPP analysis (**Supplementary Table 4**). Only seven proteins changed
202 significantly in all four replicates in melting temperature between nilotinib and imatinib with
203 a standard deviation below two degrees. For three of these proteins, we detected increased
204 ΔT_m in nilotinib-treated samples. The strongest hit was MAP kinase p38α (MAPK14) with an
205 increased ΔT_m of 6°C in nilotinib-treated samples (**Figure 3B**). The closely related isoform
206 p38γ (MAPK12) did not show significant differences (**Supplementary Figure 2A**). Also, MK3,
207 a downstream protein of p38, showed an increased ΔT_m of 2.5°C in nilotinib-treated samples
208 (**Figure 3C**). The remainder of significant proteins are shown in the **Supplementary Figure**
209 **2B-F**. To validate p38 alpha, we performed western blots of lysates from a cellular thermal
210 shift assay. The thermal denaturation temperatures for p38 alpha in DMSO and LPS-treated
211 monocytes were 50.3°C and 50.2°C, respectively. In accordance with the TPP data, the
212 thermal denaturation temperatures for p38 with nilotinib was 60.7°C, while with imatinib it
213 was 50.8°C (**Figure 3D-E**). We further performed a concentration compound range
214 experiment at 56ºC to determine the amounts of nilotinib required to alter protein thermal

stability of p38. We found that nilotinib was able to stabilize p38 at an EC50 concentration of 4.6 μM (**Supplementary Figure 2G-H**).

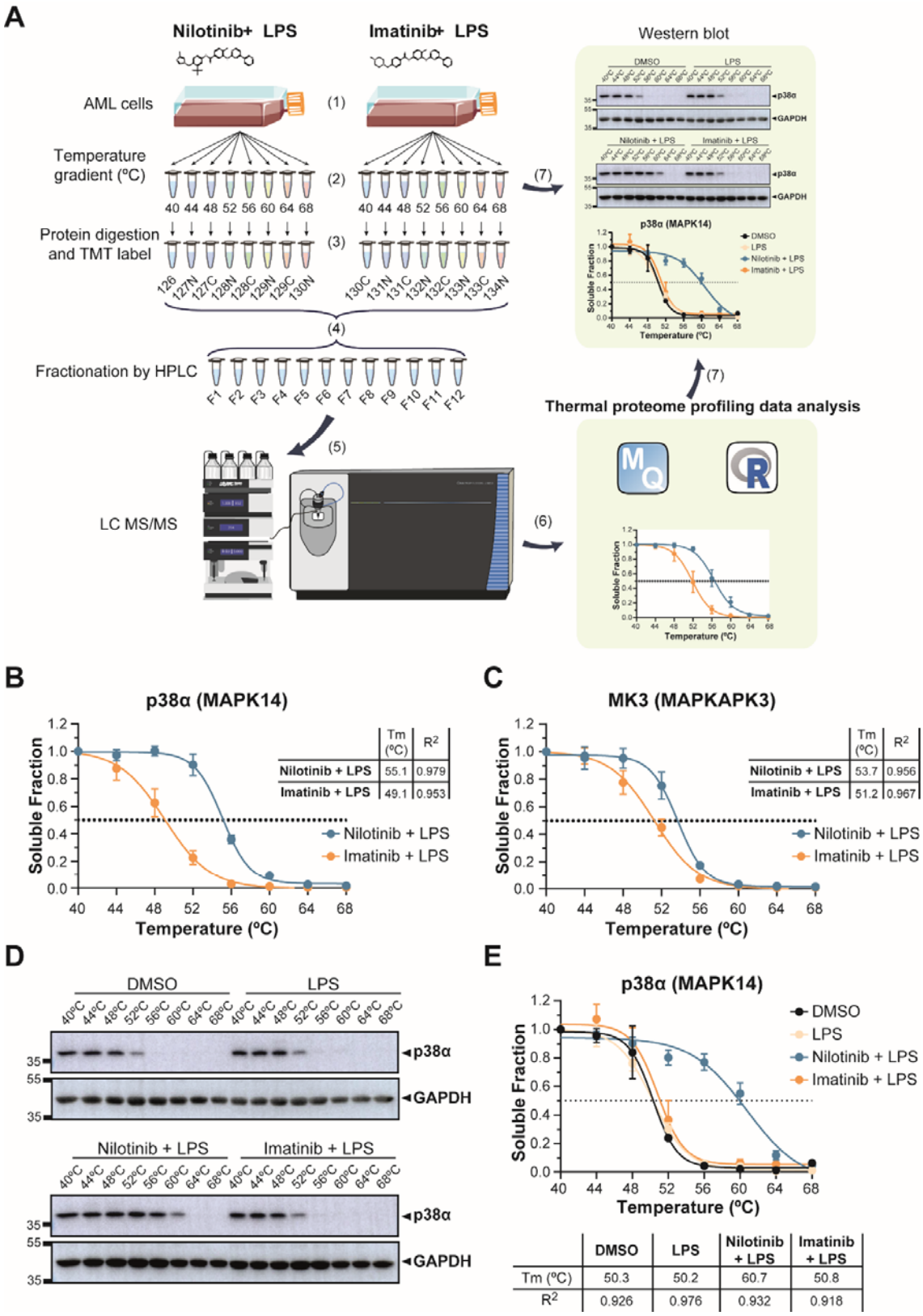
A
Nilotinib+ LPS
Imatinib+ LPS
Western blot
AML cells
(1)
Temperature gradient (ºC)
(2)
40 44 48 52 56 60 64 68
(7)
Protein digestion and TMT label
(3)
126 127N 127C 128N 128C 129N 129C 130N
130C 131N 131C 132N 132C 133N 133C 134N
(4)
Fractionation by HPLC
F1 F2 F3 F4 F5 F6 F7 F8 F9 F10 F11 F12
(7)
Thermal proteome profiling data analysis
(5)
LC MS/MS
(6)
DMSO
LPS
Nilotinib + LPS
Imatinib + LPS
p38α
GAPDH
p38α (MAPK14)
Soluble Fraction
Temperature (ºC)
B
p38α (MAPK14)
Tm (ºC)
R2
Nilotinib + LPS 55.1 0.979
Imatinib + LPS 49.1 0.953
C
MK3 (MAPKAPK3)
Nilotinib + LPS 53.7 0.956
Imatinib + LPS 51.2 0.967
D
E
DMSO
LPS
Nilotinib + LPS
Imatinib + LPS
Tm (ºC) 50.3 50.2 60.7 50.8
R2 0.926 0.976 0.932 0.918

217

Figure 3. Thermal proteome profiling (TPP) reveals stabilization of p38 alpha and MK3 in nilotinib-treated compared to imatinib-treated cells. A) Workflow of thermal proteome profiling (TPP): (1) AML cells were pre-treated with drug for 1h before adding LPS for 15 min. (2) Cells were split in 8 different tubes and heated for 3 min at a range of temperatures (40, 44, 48, 52, 56, 60, 64 and 68°C). Cells were lysed by freeze-thawing and precipitates removed by ultracentrifugation. (3) Proteins in the supernatants were digested with trypsin, labelled with 16-plex tandem mass tags (TMT) and (4) mixed. TMT-labelled peptides were fractionated using high-performance liquid chromatography (HPLC). (5) Peptides were analysed in an Orbitrap Fusion Lumos Tribrid mass spectrometer. (6) TPP data analysis was performed using MaxQuant and the computing environment R. (7) To validate the results, target proteins were analysed by western blot and melting temperatures (Tm) were calculated. **B)** Determination of the thermostability of p38 alpha (MAPK14), and **C)** MK3 (MAPKAPK3) at the indicated temperatures with 5 µM nilotinib or imatinib for one hour before 100 ng/mL LPS-treatment for up to 15 min by TPP analysis. Table insert shows melting temperature (Tm ºC) and R^2. **D)** Determination of the thermostability of p38 alpha at the indicated temperatures in vehicle control (DMSO), 100 ng/mL LPS and pre-treated with 5 µM nilotinib or imatinib for one hour before 100 ng/mL LPS-treatment for up to 15 min. GAPDH served as a loading control. **E)** Quantification of thermostability of p38 MAPK western blots from four independent experiments. Table insert shows melting temperature (Tm ºC) and R^2. Error bars represent the SEM of four biological replicates. A representative image of four replicates is shown. Relative mobilities of reference proteins (masses in kilo Daltons) are shown on the left of each blot.

In order to further understand the effect of nilotinib in preventing the inflammatory response by TLR activation in human monocytes, we used *E. coli* to stimulate and induce an inflammatory response in THP-1 cells. We used live *E. coli* rather than LPS to activate multiple inflammatory pathways and not only the pathways downstream of TLR4. Similar to LPS treatment, we were able to identify the inflammatory phenotype after exposure to *E. coli* for 24h using the MALDI-TOF MS assay (**Figure 4A**). We observed a reduction in p38

phosphorylation in stimulated monocytes treated with nilotinib similar to the specific p38 inhibitor SB202190, which eventually impacted on phosphorylation and activation of the downstream MAPK-activated protein kinase 2 (MK2) (**Figure 4B**). As Nilotinib did not affect the upstream activity of MKK3 (**Figure 4B**), it is likely that nilotinib binds p38α specifically. In order to demonstrate that the suppressive effects of nilotinib on the pro-inflammatory phenotype were mediated by inhibition of the p38 MAPK pathway in THP-1 cells, we analyzed the cytokine production mediated by p38 MAPK. In contrast to imatinib, nilotinib significantly reduced TNF-α, IL-6 and IL-1β levels and expression in monocytes stimulated with *E. coli* (**Figure 4C-E, Supplementary Figure 3**). Altogether, our results indicate that nilotinib targets p38 alpha, which inhibits its activity and affects the production of pro-inflammatory cytokines, thereby reducing inflammation.

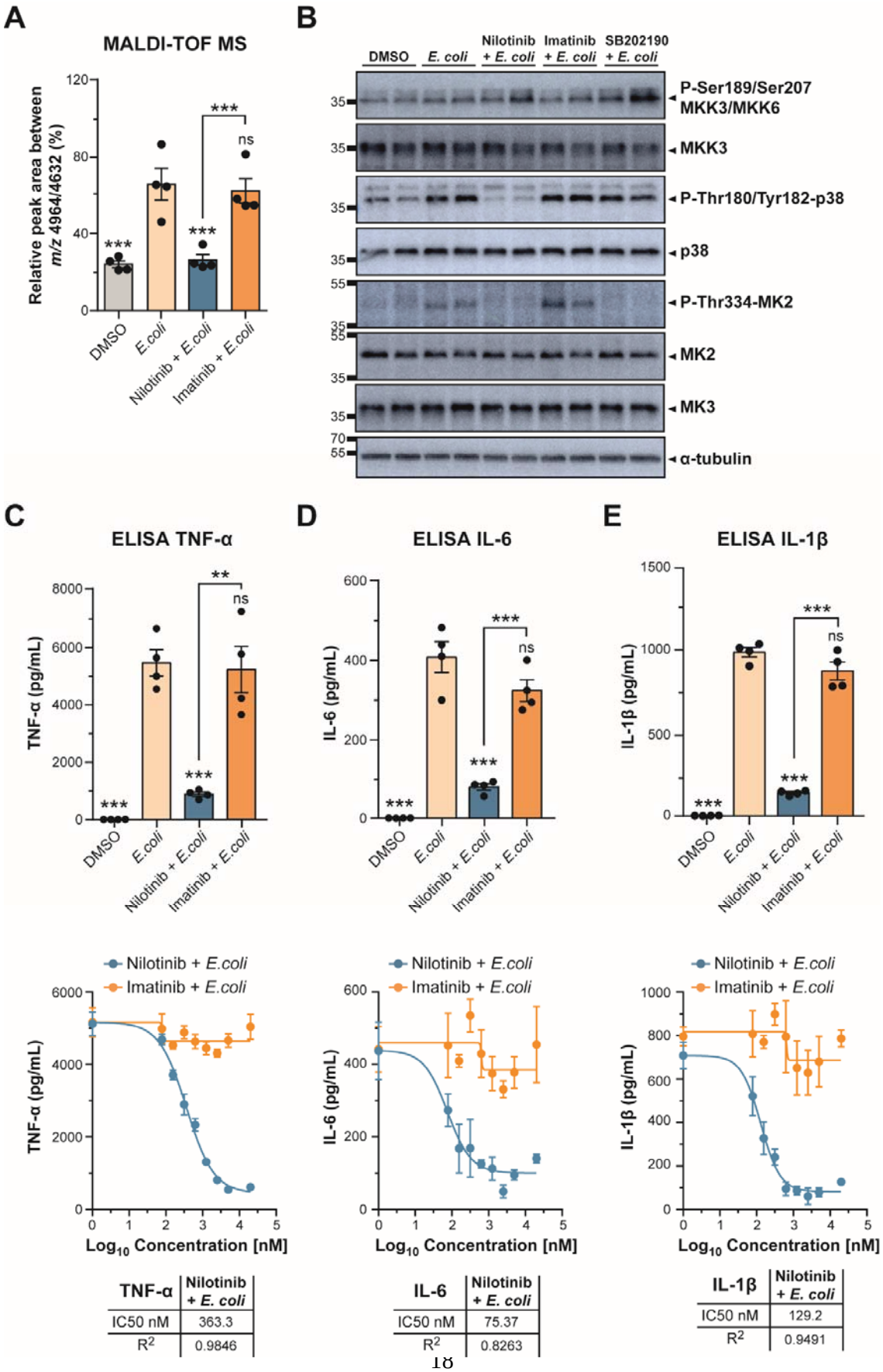

TNF-α	Nilotinib + *E. coli*
IC50 nM	363.3
R^2	0.9846

IL-6	Nilotinib + *E. coli*
IC50 nM	75.37
R^2	0.8263

IL-1β	Nilotinib + *E. coli*
IC50 nM	129.2
R^2	0.9491

259

Figure 4. Nilotinib inhibits p38 MAPK signalling. A) MALDI-TOF MS relative quantitation of the ratio *m/z* 4964 / 4632 in THP-1 cells pre-treated with DMSO, 5 µM nilotinib or imatinib for one hour before stimulation with live *E. coli* for up to 24h. **B)** Western blot analysis of the p38 MAPK pathway in THP-1 cells pre-treated with DMSO, 5 µM nilotinib, 5 µM imatinib or 10 µM SB202190 for one hour before stimulation with live *E. coli* for up to 15 min shows loss of p38 phosphorylation in response to nilotinib. Nilotinib and SB202190, but not imatinib, block phosphorylation of the downstream MK2. α-tubulin serves as a loading control. A representative image with two biological replicates of four replicates is shown. Relative mobilities of reference proteins (masses in kilo Daltons) are shown on the left of each blot. **C)** TNF-α, **D)** IL-6, and **E)** IL-1β secretion was measured by ELISA at 24h. ELISA IC50 curves are shown below. Error bars represent the SEM of four biological replicates. Significant differences between two groups were determined by a Students t-test. The statistical significance of the comparisons with *E. coli* is indicated as follows: ns, not significant; **, $P \leq 0.01$; ***, $P \leq 0.001$.

Nilotinib prevents monocyte activation.

In order to better understand differences between nilotinib and imatinib treatments on monocytes, we performed quantitative proteomics of THP-1 cells pre-treated with DMSO, 5 µM nilotinib or imatinib for one hour before stimulation with live *E. coli* for up to 24h. We identified and quantified a total of 3570 proteins of which 242 proteins showed significant differences between nilotinib and imatinib treatments (**Supplementary Table 5** and **Supplementary Figure**). Comparing differences between nilotinib and imatinib, we identified 30 significant proteins (log2 fold-change ≤ -0.6; adjusted p-value <0.05) downregulated with nilotinib (**Supplementary Table 6** and **Supplementary Figure 4C**). We found decreased levels of proteins related with cell-cell adhesion and leukocyte migration between DMSO- and nilotinib-treated cells compared to *E. coli*-stimulated and imatinib-

treated samples. Monocyte activation leads to differentiation into macrophages and also leads to an increased expression of cell adhesion proteins.[30-33] To further understand how nilotinib affected activation of monocytes and their differentiation into macrophages upon stimulation with *E. coli,* we studied cell surface differentiation and cell adhesion markers. We validated our proteomics data by showing that MMP9 and CD44 upregulation induced by *E. coli* was abolished with nilotinib but not with imatinib (**Figure 5A-B**). Furthermore, monocyte activation markers CD11c, CD14, CD49a (integrin α1) and CD54 (ICAM-1) were suppressed with nilotinib treatment but not with imatinib (**Figure 5C-F**). Also, we observed less cell adhesion with nilotinib treatment than with imatinib (**Figure 5G**). These results indicate that nilotinib inhibits the inflammatory response of monocytes under a pro-inflammatory stimulus, inhibiting their differentiation into macrophages.

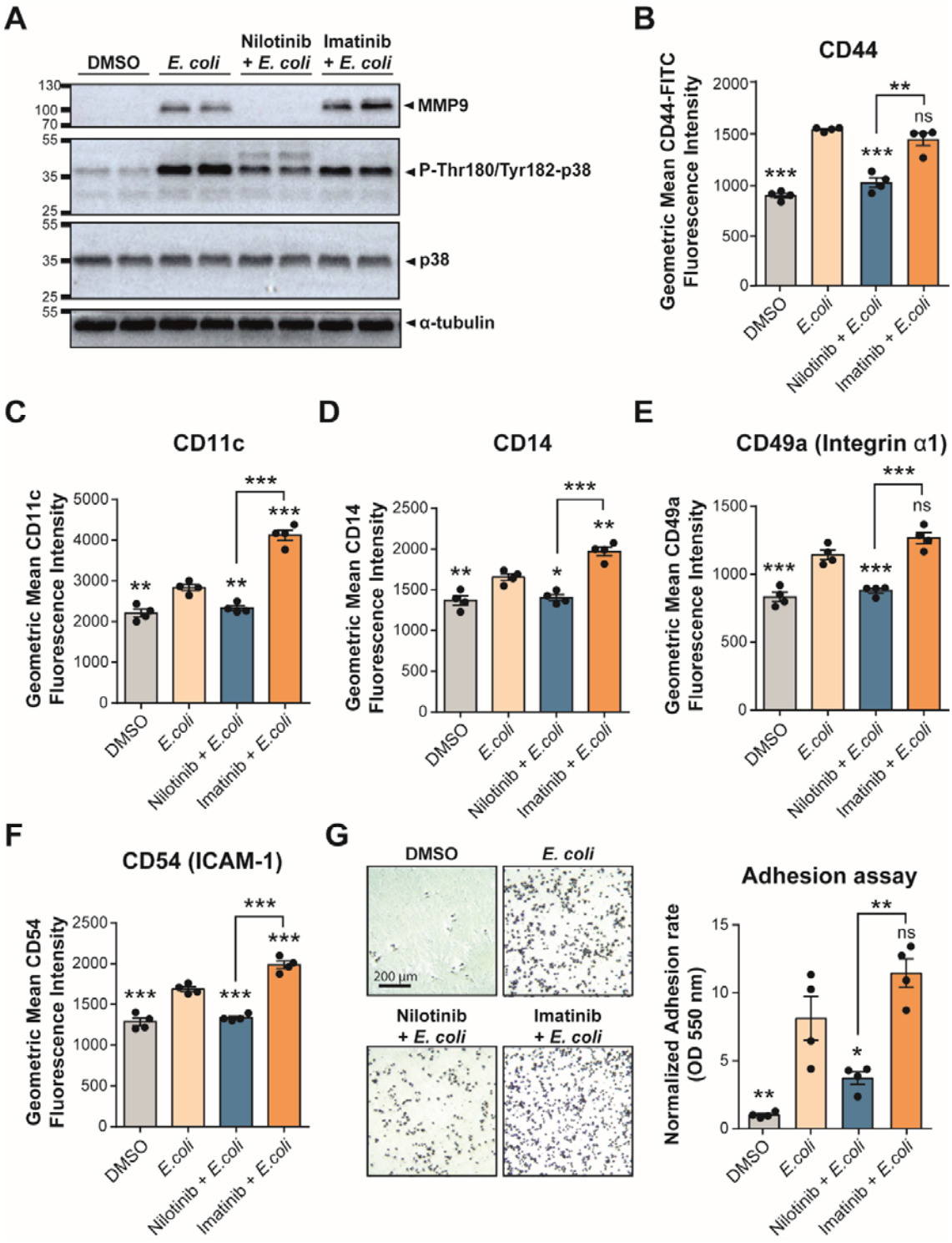

Figure 5. Nilotinib inhibits cell adhesion and monocyte activation. A) MMP9 and p38 levels in THP-1 pre-treated with 5 µM nilotinib or imatinib for one hour before stimulation with live *E. coli* for up to 24h. α-tubulin serves as a loading control. A representative image with two biological replicates of

four replicates is shown. Relative mobilities of reference proteins (masses in kilo Daltons) are shown on the left of each blot. **B)** Expression levels of CD44, **C)** CD11c, **D)** CD14, **E)** CD49a, and **F)** CD54 on the cell surface were measured by flow cytometry. **G)** Representative images of cell adhesion assay and quantification shows reduced cell adhesion upon treatment with nilotinib. Cells were stained with crystal violet and then observed by light microscopy. Optical density of dissolved crystal violet was used to evaluate the adhesion rate. Significant differences between two groups were determined by a Students t-test. The statistical significance of the comparisons with *E. coli* is indicated as follows: ns, not significant; *, $P \leq 0.05$; **, $P \leq 0.01$; ***, $P \leq 0.001$. Error bars represent the SEM of four biological replicates.

Nilotinib prevents an inflammatory response in AML and MM.

Nilotinib is a second-line therapy for CML patients who failed or were intolerant to imatinib,[23,34] but little is known about its use in other types of cancer. We performed an *in-silico* analysis of data from the Genomics of Drug Sensitivity in Cancer (GDSC) database to identify nilotinib and imatinib sensitivity in different cancer types including hematological and solid tumors. The sensitivity to nilotinib was significantly higher than that of imatinib in hematological malignancies and gastrointestinal tumors (**Supplementary Figure 5**). In particular, AML, MM and diffuse large B cell lymphomas (DLBCL) showed significant differences between the sensitivities to nilotinib and imatinib treatments (**Figure 6A**). In order to test whether nilotinib may be an effective treatment in hematological malignancies, we validated the anti-inflammatory effects of nilotinib in another monocytic AML cell line, OCI-AML2, and in a MM cell line, NCI-H929. We also observed a significant reduction in the ratio *m/z* 4964/4632 by MALDI-TOF MS in both OCI-AML2 and NCI-H929 cell lines treated with nilotinib (**Figure 6B**). Furthermore, we confirmed that nilotinib inhibits

p38 MAPK phosphorylation and subsequent MK2 phosphorylation in OCI-AML2 and NCI-H929 cell lines after exposure to *E. coli* (**Figure 6C**). Moreover, TNF-α, IL-6, and IL-1β secretion were reduced with nilotinib treatment in OCI-AML2 (**Supplementary Figure 6**). Taken together, the results show that nilotinib inhibits p38 phosphorylation during the inflammatory response, reducing the levels of cytokines such as TNF-α, IL-6 or IL-1 β (**Figure 6D**).

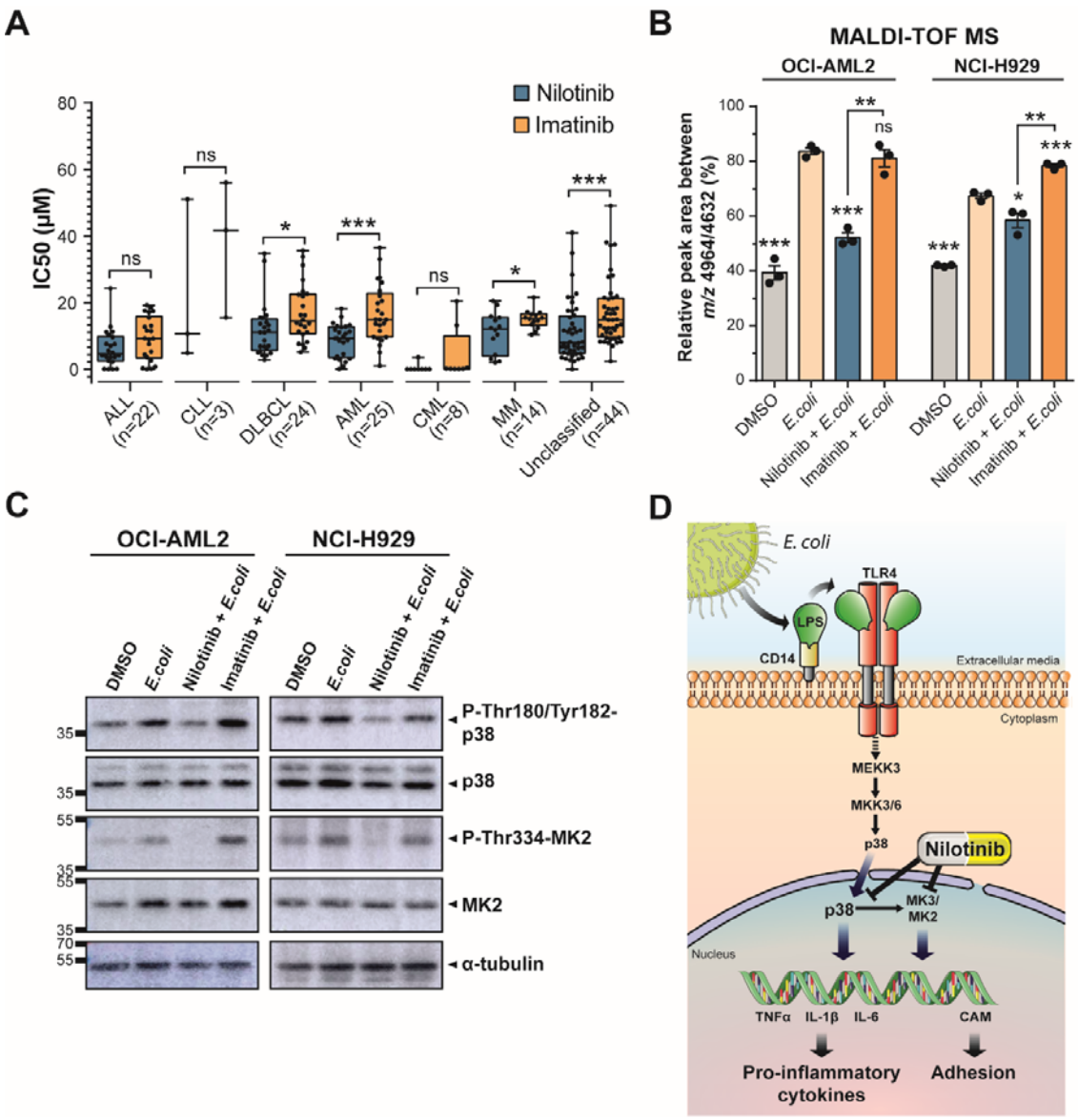

333 **Figure 6. Nilotinib reduces the inflammation phenotype in AML and MM. A)** IC50 values of nilotinib
334 and imatinib in hematological malignancies according to TCGA classification from the Genomics of
335 Drug Sensitivity in Cancer (GDSC) database. The statistical significance of the comparisons is
336 indicated as follows: ns, not significant; *, $P \leq 0.05$; ***, $P \leq 0.001$. **B)** MALDI-TOF MS relative
337 quantitation of the ratio *m/z* 4964/4632 in OCI-AML2 and NCI-H929 cells pre-treated with DMSO, 5
338 µM nilotinib or imatinib for one hour before stimulation with live *E. coli* for up to 24h. Error bars
339 represent the SEM of three biological replicates. Significant differences between two groups were
340 determined by a Students t-test. The statistical significance of the comparisons with *E. coli* is
341 indicated as follows: ns, not significant; *, $P \leq 0.05$; **, $P \leq 0.01$; ***, $P \leq 0.001$. **C)** p38 MAPK
342 pathway status in OCI-AML2 and NCI-H929 cells. α-tubulin was detected as a loading control. A
343 representative image of four replicates is shown. Relative mobilities of reference proteins (masses in
344 kilo Daltons) are shown on the left of each blot. **D)** Effect of nilotinib during pro-inflammatory
345 stimulus. Activation of TLR4 by a pro-inflammatory stimulus induces p38 MAPK signalling.
346 Nilotinib inhibits p38 phosphorylation and MK2 phosphorylation reducing the levels of
347 cytokines such as TNF-α, IL-6 or IL-1 β, and cell adhesion molecules (CAMs).
348
349 **DISCUSSION**
350 Monocytes and macrophages are major contributors to host immunity and immune
351 surveillance against inflammation.[1] Development of new high-throughput phenotypic drug
352 screening approaches is important for the identification of novel drugs for the treatment of
353 inflammation in autoimmune diseases and cancer. Here, we present a rapid and label-free
354 MALDI-TOF MS assay able to identify an inflammatory phenotype in monocytic cells, and to
355 screen for anti-inflammatory drugs. In recent years, MALDI-TOF MS has become an exciting
356 new tool for drug discovery for *in vitro* assays.[35-37] Here, we applied a screen in whole cells,
357 allowing the identification of biomolecules that provide a specific fingerprint for the

358 phenotype of the analyzed cells.[38] Two features at *m/z* 4632 and 4964 were significantly
359 altered upon inflammatory stimuli. The feature *m/z* 4964 has been previously described as a
360 biomarker to identify patients with Crohn's Disease, intestinal tuberculosis or rheumatoid
361 arthritis using MALDI MS imaging.[39,40] It has been identified as thymosin beta 4 (Tb4), a
362 small protein involved in binding and promoting actin polymerization, however it has also
363 been described as having anti-inflammatory properties.[41] Using our MALDI-TOF MS assay,
364 we identified nilotinib as a drug that prevents the inflammatory phenotype in stimulated
365 AML cells. Imatinib and nilotinib, BRC-ABL tyrosine kinase inhibitors (TKIs), are the standard
366 first-line therapy for CML.[24] However, nilotinib possesses higher potency than imatinib
367 against BCR-ABL and is active against most imatinib-resistant BCR-ABL mutations.[23] Our *in*
368 *silico* data suggest that a higher concentration of imatinib is necessary to achieve the same
369 effect elicited by nilotinib treatment in myeloid malignancies and gastrointestinal cancer;
370 such high doses could contribute to resistance or intolerance to imatinib in CML[23,34] and in
371 gastrointestinal stromal tumors as it has been observed in several clinical trials such as
372 NCT00633295, NCT00718562 or NCT00756509. Our results indicate that a lower nilotinib
373 dose already exerts anti-inflammatory effects on AML and MM. It would be interesting to
374 explore whether nilotinib has the same effect in chronic gastrointestinal inflammatory
375 diseases such as inflammatory bowel disease or Crohn's disease, which are the primary risk
376 factor for the development of gastrointestinal malignancies.[42]
377
378 Stimulation with TLR ligands activates monocytes, which leads to the production of
379 cytokines, chemokines, and mediators that are involved in inflammation.[2,43] Dysregulation
380 of TLR signalling has been linked with myeloproliferative disorders.[4,5] The bacterial surface
381 molecule LPS activates TLR4 and CD14 in monocytes, inducing pro-inflammatory (IL-1, IL-6

382 and TNF-α) and then anti-inflammatory (IL-10, soluble TNF receptor, and IL-1 receptor
383 antagonist) cytokines.[6,10] Nilotinib treatment was able to decrease the levels of IL-1β, IL-6,
384 and TNF-α cytokines secretion upon stimulation with *E. coli* in AML cells. In line with our
385 results, pre-incubation with nilotinib in murine macrophages derived from bone marrow led
386 to a decreased LPS-induced *IL-6* expression.[44] Furthermore, monocyte differentiation into
387 macrophages induces an up-regulation of CD11c and CD14 surface markers,[30,31] as well as
388 cell adhesion molecules.[32,33] Interestingly, nilotinib was able to block the upregulation of
389 CD11c, CD14, CD44, CD49a, and CD54 markers, thus reducing immune response and cell
390 adhesion of monocytes. We further found MMP9, which cleaves CD44 and induces cell
391 migration and cell-cell and cell-matrix adhesion,[45] downregulated upon nilotinib treatment.
392 Furthermore, we observed a reduction in cell adhesion in activated monocytes upon
393 nilotinib treatment, compared with imatinib. Our data therefore suggests that nilotinib may
394 not only affect inflammatory signalling and immune cell adhesion, but also differentiation
395 from monocytes into macrophages.
396
397 TLR ligation induces the formation of a signalling complex that includes IL-1R-associated
398 kinases (IRAKs) and TNFR-associated factor 6 (TRAF6), which is mediated by K63-linked
399 polyubiquitylation. This complex interacts with and activates TGFβ-activated kinase 1
400 (TAK1), a MAPK kinase kinase (MAP3K) upstream of p38α and Jun N-terminal kinases (JNKs).
401 These events in turn lead to activation of transcription factors, triggering the production of
402 cytokines and chemokines.[9,46] TPP analysis identified p38α as a main off-target of nilotinib,
403 when compared with imatinib. Nilotinib has been reported to inhibit p38α and p38γ, in an *in*
404 *vitro* kinase assay and may stabilize p38α through direct interaction, as it has been observed
405 in vascular endothelial cells.[47] Furthermore, it was shown that nilotinib was able to block

p38 and JNK activation in an *in vivo* model of ischemic reperfusion injury, leading to decreased cytokine production and modulated leukocyte recruitment.[48] However, we did not find any evidence for p38γ or JNK inhibition in our experiments, suggesting remarkable specificity for the 38α isoform. Furthermore, our results showed that nilotinib interferes with the downstream MAPK signalling pathway comparable to a specific p38 inhibitor. The potential of p38 MAPK inhibitors was initially explored within inflammatory conditions such as rheumatoid arthritis and Crohn's disease, but early studies demonstrated poor clinical efficacy and unacceptable side effects.[49] This suggests that nilotinib may be considered for additional applications outside of cancer, particularly as it is well tolerated by patients and has few side effects. [23,34] Within the cancer field, it appears that the anti-inflammatory off-target effects from nilotinib may be beneficial as seen in tumors co-treated with doxorubicin and vincristine.[50,51] Consistent with these results, nilotinib – but not imatinib – can reduce the inflammation in human monocytes-derived from AML and other myeloid cells.

Our study provides a valuable tool to discover new anti-inflammatory drugs using MALDI-TOF MS, as we demonstrate here for nilotinib. We show that nilotinib inhibits p38α, prevents its phosphorylation and subsequent activation, affecting the phosphorylation of downstream signalling targets and, ultimately preventing the transcription of pro-inflammatory genes, cell adhesion markers and innate immunity markers. In consequence, nilotinib may have therapeutic potential through the inhibition of p38 MAPK pathway in inflammatory diseases as well as in myeloid malignancies such as myeloid leukemia and multiple myeloma.

ACKNOWLEDGEMENTS

We would like to thank the animal staff at Newcastle University's Comparative Biology Centre, and Akshada Gajbhiye, Abeer Dannoura, Julien Peltier, and Anetta Härtlova for their technical support. This research was partly funded by a Wellcome Trust Investigator Award (215542/Z/19/Z) and generous start-up funding of Newcastle University to M.T. R.E.H. was funded by an iCASE studentship by the BBSRC and Bruker Daltonics. M.E.D. is a Marie Sklodowska Curie Fellow within the European Union's Horizon 2020 research and innovation programme under the Marie Skłodowska-Curie grant agreement No. 890296. For the purpose of Open Access, the author has applied a CC BY public copyright license to any Author Accepted Manuscript version arising from this submission.

AUTHORSHIP CONTRIBUTIONS

R.E.H. and J.L.M.-R. are co-first authors. J.L.M.-R. performed cellular thermal shift assay, ELISA and flow cytometry. R.E.H. and M.E.D. performed MALDI-TOF MS experiments. J.L.M.-R. and T.H. performed LFQ and TMT mass spectrometry-based proteomics experiments. T.H. analyzed TPP experiments. J.L.M.-R. and J.I. performed and analyzed RTqPCR assays. B.S. provided drug panel. M.T. conceived the original idea and provided supervision. J.L.M.-R., R.E.H., and M.T. wrote the manuscript. All authors provided critical feedback and helped shape the research, analysis and manuscript.

SUPPLEMENTAL INFORMATION

The online version of this article contains supplementary data.

REFERENCES

1 Gordon, S. & Taylor, P. R. Monocyte and macrophage heterogeneity. *Nat Rev Immunol* **5**, 953-964, doi:10.1038/nri1733 (2005).

2 Stuhlmuller, B. *et al.* Identification of known and novel genes in activated monocytes from patients with rheumatoid arthritis. *Arthritis Rheum* **43**, 775-790, doi:10.1002/1529-0131(200004)43:4<775::AID-ANR8>3.0.CO;2-7 (2000).

3 Binder, S., Luciano, M. & Horejs-Hoeck, J. The cytokine network in acute myeloid leukemia (AML): A focus on pro- and anti-inflammatory mediators. *Cytokine Growth Factor Rev* **43**, 8-15, doi:10.1016/j.cytogfr.2018.08.004 (2018).

4 Hemmati, S., Haque, T. & Gritsman, K. Inflammatory Signaling Pathways in Preleukemic and Leukemic Stem Cells. *Front Oncol* **7**, 265, doi:10.3389/fonc.2017.00265 (2017).

5 Monlish, D. A., Bhatt, S. T. & Schuettpelz, L. G. The Role of Toll-Like Receptors in Hematopoietic Malignancies. *Front Immunol* **7**, 390, doi:10.3389/fimmu.2016.00390 (2016).

6 Takeuchi, O. *et al.* Differential roles of TLR2 and TLR4 in recognition of gram-negative and gram-positive bacterial cell wall components. *Immunity* **11**, 443-451, doi:10.1016/s1074-7613(00)80119-3 (1999).

7 Takeda, K. & Akira, S. Toll-like receptors in innate immunity. *Int Immunol* **17**, 1-14, doi:10.1093/intimm/dxh186 (2005).

8 Kim, E. K. & Choi, E. J. Pathological roles of MAPK signaling pathways in human diseases. *Biochim Biophys Acta* **1802**, 396-405, doi:10.1016/j.bbadis.2009.12.009 (2010).

9 Suzuki, T. *et al.* Different involvement of the MAPK family in inflammatory regulation in human pulmonary microvascular endothelial cells stimulated with LPS and IFN-gamma. *Immunobiology* **223**, 777-785, doi:10.1016/j.imbio.2018.08.003 (2018).

10 Mogensen, T. H. Pathogen recognition and inflammatory signaling in innate immune defenses. *Clin Microbiol Rev* **22**, 240-273, Table of Contents, doi:10.1128/CMR.00046-08 (2009).

11 Inglese, J. *et al.* High-throughput screening assays for the identification of chemical probes. *Nat Chem Biol* **3**, 466-479, doi:10.1038/nchembio.2007.17 (2007).

12 Neefjes, J. & Dantuma, N. P. Fluorescent probes for proteolysis: tools for drug discovery. *Nat Rev Drug Discov* **3**, 58-69, doi:10.1038/nrd1282 (2004).

13 Adegbola, S. O., Sahnan, K., Warusavitarne, J., Hart, A. & Tozer, P. Anti-TNF Therapy in Crohn's Disease. *Int J Mol Sci* **19**, doi:10.3390/ijms19082244 (2018).

14 Dulai, P. S. & Sandborn, W. J. Next-Generation Therapeutics for Inflammatory Bowel Disease. *Curr Gastroenterol Rep* **18**, 51, doi:10.1007/s11894-016-0522-0 (2016).

15 Li, P., Zheng, Y. & Chen, X. Drugs for Autoimmune Inflammatory Diseases: From Small Molecule Compounds to Anti-TNF Biologics. *Front Pharmacol* **8**, 460, doi:10.3389/fphar.2017.00460 (2017).
16 Guitot, K. *et al.* A direct label-free MALDI-TOF mass spectrometry based assay for the characterization of inhibitors of protein lysine methyltransferases. *Anal Bioanal Chem* **409**, 3767-3777, doi:10.1007/s00216-017-0319-5 (2017).
17 Heap, R. E. *et al.* Identifying Inhibitors of Inflammation: A Novel High-Throughput MALDI-TOF Screening Assay for Salt-Inducible Kinases (SIKs). *SLAS Discov* **22**, 1193-1202, doi:10.1177/2472555217717473 (2017).
18 De Cesare, V. *et al.* The MALDI-TOF E2/E3 Ligase Assay as Universal Tool for Drug Discovery in the Ubiquitin Pathway. *Cell Chem Biol* **25**, 1117-1127 e1114, doi:10.1016/j.chembiol.2018.06.004 (2018).
19 Bosshart, H. & Heinzelmann, M. THP-1 cells as a model for human monocytes. *Ann Transl Med* **4**, 438, doi:10.21037/atm.2016.08.53 (2016).
20 Clark, K. *et al.* Novel cross-talk within the IKK family controls innate immunity. *Biochem J* **434**, 93-104, doi:10.1042/BJ20101701 (2011).
21 Tan, L. *et al.* Discovery of type II inhibitors of TGFbeta-activated kinase 1 (TAK1) and mitogen-activated protein kinase kinase kinase kinase 2 (MAP4K2). *J. Med. Chem.* **58**, 183-196, doi:10.1021/jm500480k (2015).
22 Malik, N. *et al.* Suppression of interferon beta gene transcription by inhibitors of bromodomain and extra-terminal (BET) family members. *Biochem. J.* **468**, 363-372, doi:10.1042/BJ20141523 (2015).
23 Wei, G., Rafiyath, S. & Liu, D. First-line treatment for chronic myeloid leukemia: dasatinib, nilotinib, or imatinib. *J Hematol Oncol* **3**, 47, doi:10.1186/1756-8722-3-47 (2010).
24 Pan, P. *et al.* Systematic Review and Meta-Analysis of -New-Generation Tyrosine Kinase Inhibitors versus Imatinib for Newly Diagnosed Chronic Myeloid Leukemia. *Acta Haematol*, 1-13, doi:10.1159/000501537 (2019).
25 Franken, H. *et al.* Thermal proteome profiling for unbiased identification of direct and indirect drug targets using multiplexed quantitative mass spectrometry. *Nat Protoc* **10**, 1567-1593, doi:10.1038/nprot.2015.101 (2015).
26 Mateus, A. *et al.* Thermal proteome profiling for interrogating protein interactions. *Mol Syst Biol* **16**, e9232, doi:10.15252/msb.20199232 (2020).
27 Miettinen, T. P. *et al.* Thermal proteome profiling of breast cancer cells reveals proteasomal activation by CDK4/6 inhibitor palbociclib. *EMBO J* **37**, doi:10.15252/embj.201798359 (2018).
28 Becher, I. *et al.* Thermal profiling reveals phenylalanine hydroxylase as an off-target of panobinostat. *Nat Chem Biol* **12**, 908-910, doi:10.1038/nchembio.2185 (2016).
29 Savitski, M. M. *et al.* Tracking cancer drugs in living cells by thermal profiling of the proteome. *Science* **346**, 1255784, doi:10.1126/science.1255784 (2014).
30 Ma, W. *et al.* The p38 mitogen-activated kinase pathway regulates the human interleukin-10 promoter via the activation of Sp1 transcription factor in

lipopolysaccharide-stimulated human macrophages. *J Biol Chem* **276**, 13664-13674, doi:10.1074/jbc.M011157200 (2001).

31 Chen, R. F., Wang, L., Cheng, J. T. & Yang, K. D. Induction of IFNalpha or IL-12 depends on differentiation of THP-1 cells in dengue infections without and with antibody enhancement. *BMC Infect Dis* **12**, 340, doi:10.1186/1471-2334-12-340 (2012).

32 Kounalakis, N. S. & Corbett, S. A. Lipopolysaccharide transiently activates THP-1 cell adhesion. *J Surg Res* **135**, 137-143, doi:10.1016/j.jss.2005.12.018 (2006).

33 Park, G. S. & Kim, J. H. LPS Up-Regulates ICAM-1 Expression in Breast Cancer Cells by Stimulating a MyD88-BLT2-ERK-Linked Cascade, Which Promotes Adhesion to Monocytes. *Mol Cells* **38**, 821-828, doi:10.14348/molcells.2015.0174 (2015).

34 Sasaki, K. *et al.* Frontline therapy with high-dose imatinib versus second generation tyrosine kinase inhibitor in patients with chronic-phase chronic myeloid leukemia - a propensity score analysis. *Haematologica* **101**, e324-327, doi:10.3324/haematol.2015.139089 (2016).

35 De Cesare, V. *et al.* High-throughput matrix-assisted laser desorption/ionization time-of-flight (MALDI-TOF) mass spectrometry-based deubiquitylating enzyme assay for drug discovery. *Nat. Protoc.* **15**, 4034-4057, doi:10.1038/s41596-020-00405-0 (2020).

36 Simon, R. P. *et al.* MALDI-TOF-Based Affinity Selection Mass Spectrometry for Automated Screening of Protein-Ligand Interactions at High Throughput. *SLAS Discov* **26**, 44-57, doi:10.1177/2472555220959266 (2021).

37 Winter, M. *et al.* Automated MALDI Target Preparation Concept: Providing Ultra-High-Throughput Mass Spectrometry-Based Screening for Drug Discovery. *SLAS Technol* **24**, 209-221, doi:10.1177/2472630318791981 (2019).

38 Heap, R. E., Segarra-Fas, A., Blain, A. P., Findlay, G. M. & Trost, M. Profiling embryonic stem cell differentiation by MALDI TOF mass spectrometry: development of a reproducible and robust sample preparation workflow. *Analyst* **144**, 6371-6381, doi:10.1039/c9an00771g (2019).

39 Kriegsmann, M. *et al.* MALDI MS imaging as a powerful tool for investigating synovial tissue. *Scand J Rheumatol* **41**, 305-309, doi:10.3109/03009742.2011.647925 (2012).

40 Zhang, F. *et al.* Exploration of Serum Proteomic Profiling and Diagnostic Model That Differentiate Crohn's Disease and Intestinal Tuberculosis. *PLoS One* **11**, e0167109, doi:10.1371/journal.pone.0167109 (2016).

41 Holzlechner, M. *et al.* In Situ Characterization of Tissue-Resident Immune Cells by MALDI Mass Spectrometry Imaging. *J. Proteome Res.* **16**, 65-76, doi:10.1021/acs.jproteome.6b00610 (2017).

42 Boyapati, R. K., Rossi, A. G., Satsangi, J. & Ho, G. T. Gut mucosal DAMPs in IBD: from mechanisms to therapeutic implications. *Mucosal Immunol* **9**, 567-582, doi:10.1038/mi.2016.14 (2016).

43 Yang, R. B. *et al.* Toll-like receptor-2 mediates lipopolysaccharide-induced cellular signalling. *Nature* **395**, 284-288, doi:10.1038/26239 (1998).
44 Wong, J. *et al.* Small molecule kinase inhibitors block the ZAK-dependent inflammatory effects of doxorubicin. *Cancer Biol Ther* **14**, 56-63, doi:10.4161/cbt.22628 (2013).
45 Chetty, C. *et al.* MMP-9 induces CD44 cleavage and CD44 mediated cell migration in glioblastoma xenograft cells. *Cell Signal* **24**, 549-559, doi:10.1016/j.cellsig.2011.10.008 (2012).
46 Arthur, J. S. & Ley, S. C. Mitogen-activated protein kinases in innate immunity. *Nat Rev Immunol* **13**, 679-692, doi:10.1038/nri3495 (2013).
47 Hadzijusufovic, E. *et al.* Nilotinib-induced vasculopathy: identification of vascular endothelial cells as a primary target site. *Leukemia* **31**, 2388-2397, doi:10.1038/leu.2017.245 (2017).
48 Ocuin, L. M. *et al.* Nilotinib protects the murine liver from ischemia/reperfusion injury. *J Hepatol* **57**, 766-773, doi:10.1016/j.jhep.2012.05.012 (2012).
49 Fisk, M., Gajendragadkar, P. R., Maki-Petaja, K. M., Wilkinson, I. B. & Cheriyan, J. Therapeutic potential of p38 MAP kinase inhibition in the management of cardiovascular disease. *Am J Cardiovasc Drugs* **14**, 155-165, doi:10.1007/s40256-014-0063-6 (2014).
50 Dent, P. The flip side of doxorubicin: Inflammatory and tumor promoting cytokines. *Cancer Biol Ther* **14**, 774-775, doi:10.4161/cbt.26125 (2013).
51 Wong, J., Tran, L. T., Magun, E. A., Magun, B. E. & Wood, L. J. Production of IL-1beta by bone marrow-derived macrophages in response to chemotherapeutic drugs: synergistic effects of doxorubicin and vincristine. *Cancer Biol Ther* **15**, 1395-1403, doi:10.4161/cbt.29922 (2014).

METHODS

Compounds

LPS and SB202190 were purchased from Sigma-Aldrich; Pam2CSK4 and Pam3CSK4 from Invitrogen; IFN-γ from PeproTech; and nilotinib, imatinib, NG-25, MRT67307, and the other compounds from Supplementary Table 1 were provided by LifeArc.

Cell culture.

615 Acute myeloid leukemia-derived cell lines THP-1 (ATCC) and OCI-AML2 (DSMZ), and multiple
616 myeloma-derived cell lines NCI-H929 (ATCC) were cultured at 37°C in a humidified 5% CO_2
617 atmosphere. ATCC and DSMZ routinely perform cell line authentication, using short tandem
618 repeat profiling as a procedure. Cell experimentation was always performed within a period
619 not exceeding six months after resuscitation in mycoplasma-free culture conditions.
620
621 **Blind drug screening.**
622 One million THP-1 cells/mL were incubated with each compound (**Supplementary Table 1**)
623 at 5 µM for one hour in technical triplicates before stimulation with 100 ng/mL LPS for 24h.
624 Compounds were staggered into 8 sets each with individual positive (NG-25) and negative
625 controls (MRT67307) to enable maximum relative peak area calculations. This screening
626 process was repeated in three biological replicates.
627
628 **Cell infection with *E. coli*.**
629 The DH5α strain of *E. coli* bacteria (Invitrogen) was harvested during mid-log phase.
630 Mammalian cells were infected with a multiplicity of infection of 2. The cells with bacteria
631 were centrifuged at 500 xg for 5 min at 37°C and incubated at 37°C in 5% CO_2 for bacterial
632 uptake for 15 min or 30 min. Thirty min post-infection, cells were washed once with PBS and
633 incubated for 1h with 100 µg/mL gentamicin to kill extracellular bacteria. Then, the cells
634 were washed with PBS twice and the media replaced with 20 µg/mL gentamicin for the
635 remainder of the experiment.
636
637 **Sample preparation for MALDI-TOF MS and data analysis.**

Cell pellets were frozen on dry ice, then thawed and washed with 100 mM Tris-HCl, pH 7.5 and centrifuged at 1,000 xg for 10 min at 4°C. 2,500 cells were spotted on target with 10 mg/mL α-cyano-4-cinnamic acid in 50% acetonitrile, 0.1% trifluoroacetic acid. Automated target spotting was performed using a Mosquito liquid handling robot (TTP Labtech). A RapifleX PharmaPulse MALDI TOF/TOF mass spectrometer (Bruker Daltonics) equipped with a Smartbeam 3D laser was used in positive ion mode. Samples were acquired in automatic mode (AutoXecute; Bruker Daltonics), totaling 10,000 shots at a 10 kHz frequency per spot. A random walk pattern (complete sample) on spot laser ablation pattern was used with an M5 Smart beam Parameter at a 45 µm × 45 µm scan range. Spot diameter was limited to 2,000 µm and a random walk pattern movement enabled at 1000 shots per raster position. Ionization was achieved using a laser power of 75% (laser attenuator offset 14%, range 30%) with a detector gain of ×6.8 in the mass range of *m/z* 2,000-20,000 with a mass suppression up to m/z 1,600. Samples were analyzed in a linear geometry with optimized voltages for ion sources (ion source 1, 20 kV; pulsed ion extraction 1.3 kV), lens (8.6 kV), and a pulsed ion extraction of 180 ns. A novel 10-bit digitizer was used at a sampling rate of 1.25 GS/s. Raw data were processed first by a TopHat baseline subtraction followed by smoothing with a SavitzkyGolay algorithm. MALDI-TOF spectra were processed by FlexAnalysis Batch Process (Compass 2.0). Spectra-based PCA plots were generated using ClinPro Tools (Bruker Daltonics). A normalized relative peak area was used to measure a pro-inflammatory response between *m/z* 4632 and 4963 and was calculated with the following equation:

$$Normalised\ peak\ area\ ratio = \left(\left(\frac{4963\ peak\ area}{4632\ peak\ area} \right) / (LPS\ treated) \right) \times 100$$

658 This method of intra-spectra quantification[1] was robust over ten different passages, where
659 we were able to quantify the inflammatory response by MALDI-TOF MS with Z'>0.5 and
660 $P \leq 0.001$.
661
662 **Quantitative RT-PCR.**
663 RNA was extracted using Trizol (Thermo Fisher Scientific). Real-time RT-qPCR from total RNA
664 in two steps, was performed with a QuantiTect reverse transcription kit (Qiagen), and
665 QuantiTect SYBR green kit (Qiagen) using a StepOne Applied Biosystems real-time PCR
666 system (Thermo Fisher Scientific). Expression values of *GAPDH* and *TBP* genes in the same
667 samples were used for normalization, using the $2^{-\Delta\Delta CT}$ method. The following primers were
668 used: *GAPDH*, forward: GTCTCCTCTGACTTCAACAGCG and, reverse:
669 ACCACCCTGTTGCTGTAGCCAA; *IL-6*, forward: GCCCAGCTATGAACTCCTTCT and, reverse:
670 CTTCTCCTGGGGGTACTGG; *TBP*, forward: GAGTTCCAGCGCAAGGGTTT, and, reverse:
671 GGGTCAGTCCAGTGCCATA; *TNF-α*, forward: AAACTCATGAGCAGTCTGCA, and reverse:
672 AGGAGATCTTCAGTTTCGGAGG.
673
674 **ELISA.**
675 Cell culture supernatant was collected at 24h post-treatment. TNF-a, IL-6, and IL-1β were
676 measured by DuoSet ELISA kits (R&D Systems). Absorbance from four biological replicates at
677 450 nm was measured with the correction wavelength set at 540 nm using SpectraMax® M3
678 microplate reader (Molecular Devices).
679
680 **Western blot.**

681 Cells were lysed using 5% SDS supplemented with Protease Inhibitor Cocktail and
682 Phosphatase Inhibitor Cocktail 2 (Sigma-Aldrich). The following antibodies were purchased
683 from Cell Signaling Technology (Danvers): MK2 (#3042), Thr-334-P-MK2 (#3041), MK3
684 (#7421), MKK3 (#8535), Ser189-P-MKK3/Ser207-P-MKK6 (#12280), p38 MAPK (#9212), p38α
685 MAPK (#9218), p38γ MAPK (#2307) Thr180/Tyr182-P-p38 MAPK (#4511), MPP9 (#13667),
686 anti-rabbit IgG-HRP (#7074), and anti-mouse IgG (#7076). GAPDH (sc-47724) was from Santa
687 Cruz, and α-Tubulin (T9026) was from Sigma-Aldrich. Amersham Imager 600 digital imaging
688 system (GE Healthcare) was used for image acquisition.
689
690 **Flow cytometry.**
691 Cell surface staining was performed by direct immunofluorescent assay with fluorescent-
692 conjugated antibodies: CD11c-APC (#17-0114-82), CD14-AF700 (#56-0149-42), and CD54-
693 FITC (#11-0541-82) from Thermo Fisher; CD49a-PE (#562115) and CD44-FITC (#338803) from
694 BD Biosciences; and corresponding isotype control antibodies, for 30 min at 4°C in PBS with
695 1% FBS, 1% BSA and 1% human serum (Sigma) to block Fc receptors. Cells were analyzed in a
696 FACSCanto II flow cytometer (Becton-Dickinson). The results were analyzed using FlowJo.
697
698 **Adhesion assay.**
699 Cells were washed twice with PBS before being fixed with 4% paraformaldehyde for 15 min.
700 Then, cells were incubated with 5 mg/ml Crystal violet for 10 min before lysis with 2% SDS
701 for 30 min. Absorbance from four biological replicates at 550 nm was measured using a
702 SpectraMax® M3 microplate reader (Molecular Devices). Micrographs were acquired with an
703 inverted microscope Axio Vert.A1 FL LED (Zeiss, Cambridge).
704

705 **Cellular thermal shift assay.**

706 Cells were treated with 5 µM of nilotinib or imatinib for one hour, then 100 ng/mL LPS was
707 added for 15 min. Cells were washed with PBS supplemented with cOmplete, EDTA-free
708 Protease Inhibitor Cocktail (Sigma-Aldrich), 1.2 mM sodium molybdate, 1 mM sodium
709 orthovanadate, 4 mM sodium tartrate dihydrate, 5 mM glycerophosphate, and 20 mM N-
710 ethylmaleimide; then separated into 8 fractions for thermal profiling. Fractions were heated
711 at 40, 44, 48, 52, 56, 60, 64 and 68°C for 3 min. For concentration compound range
712 experiments, cells were treated with 0.1, 0.5, 1, 5 or 10 µM of nilotinib or imatinib for 1h
713 before treatment with 100 ng/mL LPS for 15 min. Cells were heated at 56°C for 3 min.
714 Samples were lysed with four freeze-thaw cycles using dry ice and a thermo block at 35°C.
715 Cell lysates were centrifuged at 20,000 xg for 2h at 4°C to separate protein aggregates from
716 soluble proteins. Supernatants were collected and used for western blot and mass
717 spectrometry.

718

719 **Sample preparation for LC-MS/MS and label-free quantification (LFQ) data analysis.**

720 Samples were prepared for mass spectrometry using S-Trap micro columns (Protifi)
721 according to the manufacturer's recommended protocol. Proteins were reduced with 20
722 mM TCEP at 37°C for 30 min and alkylated with 20 mM N-ethylmaleimide in the dark for 30
723 min. A ratio of 1:10 wt:wt Trypsin TPCK Treated (Worthington-Biochem) was used to digest
724 the samples for 2h at 47°C. Eluted peptides were dried down and resuspended in loading
725 buffer (2% acetonitrile, 0.1% trifluoroacetic acid). Peptide samples were injected on a
726 Dionex Ultimate 3000 RSLC (Thermo Fisher Scientific) connected to an Orbitrap Fusion
727 Lumos Tribrid mass spectrometer (Thermo Fisher Scientific). Samples were injected on a
728 PepMap 100 C18 LC trap column (300 µm ID x 5 mm, 5 µm, 100 Å) followed by separation

729 on an EASY-Spray column (50 cm x 75 µm ID, PepMap C18, 2 µm, 100 Å) (Thermo Fisher
730 Scientific). Buffer A consisted of water containing 0.1% FA and Buffer B of 80% acetonitrile
731 containing 0.1% FA. Peptides were separated with a linear gradient of 3-35% Buffer B over
732 180 min followed by a step from 35-90% Buffer B in 0.5 min at 250 nL/min and held at 90%
733 for 4 min. The gradient was then decreased to 3% Buffer B in 0.5 min at 250 nL/min, and the
734 column equilibrated for 10 min before the next injection. Column temperature was
735 controlled at 45°C. The Orbitrap Fusion Lumos Tribrid mass spectrometer was operated in
736 data-dependent, positive ion mode. Full scan spectra were acquired in the range of *m/z* 400
737 to 1,600, at a resolution of 120,000, with an automatic gain control (AGC) target of $4x10^5$
738 and a maximum injection time of 50 ms. The Orbitrap was operated in 'stop speed' to
739 maintain a 3 sec fixed duty cycle. The most intense precursor ions were isolated with a
740 quadrupole mass filter width of 1.6 *m/z* and higher-energy collision-induced dissociation
741 (HCD) fragmentation was performed in one-step collision energy of 30%. Detection of
742 MS/MS fragments was acquired in the linear ion trap in rapid scan mode with an AGC target
743 of $1x10^4$ ions and a maximum injection time of 45 ms. An electrospray voltage of 2.0 kV and
744 capillary temperature of 275°C, with no sheath and auxiliary gas flow, was used.

745 All discovery proteomics RAW mass spectra were analyzed using MaxQuant (version
746 1.6.10.43)[2] and searched against a SwissProt Homo sapiens database (containing 42,347
747 database entries with isoforms; downloaded on 21 April 2020). Trypsin/P was set as
748 proteolytic enzyme, N-ethylmaleimide on cysteine was set as fixed modification, and
749 methionine oxidation and acetylation of protein N-termini was set as variable modifications.
750 Two missed cleavages were allowed. A protein and peptide false discovery rate (FDR) of less
751 than 1% was employed in MaxQuant. LFQ data analysis was performed using Perseus
752 (version 1.6.2.3).[3] Reverse hits, contaminants and proteins only identified by site were

753 removed before downstream statistical and bioinformatics analysis. LFQ intensity data were
754 transformed (log 2) and filtered to contain at least two unique peptides and at least three
755 valid values in one group for comparisons. Significance testing was carried out using a two-
756 tailed unpaired Student's t-test and multiple hypothesis testing was controlled using the
757 Benjamini-Hochberg FDR threshold of p-value <0.05. Gene ontology term enrichments were
758 performed within DAVID (version 6.8).[4]
759
760 **Thermal proteome profiling (TPP) and data analysis.**
761 Isobaric labeling of peptides was performed using the 16-plex tandem mass tag (TMT)
762 reagents (Thermo Fisher Scientific) (**Supplementary Table 2**), according to the manufacturer
763 recommended protocol. According to the different temperature points, labeled peptides
764 were combined and desalted with C18 Macro Spin Columns (Harvard Apparatus, Holliston,
765 MA, USA). The TMT-labeled samples were subjected to fractionation using basic-pH
766 reversed-phase liquid chromatography on a Dionex Ultimate 3000 HPLC system (Thermo
767 Fisher Scientific) using a Gemini C18 column (250 mm × 3 mm, 3 µm, 110 Å; Phenomenex).
768 Buffer A consisted of 20 mM ammonium formate pH 8.0 and Buffer B of 100% acetonitrile.
769 Peptides were fractionated using a linear gradient of 1-49% buffer B over 49 min at 250
770 nl/min. Twelve fractions were dried under vacuum centrifugation and resuspended in 2%
771 acetonitrile with 0.1% TFA for LC-MS/MS analysis. Labeled peptide samples were injected on
772 a Dionex Ultimate 3000 RSLC (Thermo Fisher Scientific) connected to an Orbitrap Fusion
773 Lumos Tribrid mass spectrometer (Thermo Fisher Scientific). Buffer A consisted of water
774 containing 0.1% FA and Buffer B of 80% acetonitrile containing 0.1% FA. Peptides were
775 separated with a linear gradient of 3-35% Buffer B over 180 min followed by a step from 35-
776 90% Buffer B in 0.5 min at 250 nL/min and held at 90% for 4 min. The gradient was then

decreased to 3% Buffer B in 0.5 min at 250 nL/min, and the column equilibrated for 10 min before the next injection. The scan sequence began with an MS1 spectrum (Orbitrap analysis; resolution 120,000; mass range *m/z* 375-1500; automatic gain control (AGC) target 4x10E5; maximum injection time 50 ms). MS2 analysis consisted of collision-induced dissociation (CID); AGC 1x10E4; normalized collision energy (NCE) of 30%; maximum injection time 50 ms; and isolation window of 0.7. Following acquisition of each MS2 spectrum, MS3 precursors were fragmented by high energy collision-induced dissociation (HCD) and analyzed using the Orbitrap (NCE 55%; AGC 5x10E4; maximum injection time 86 ms, resolution was 50,000) and synchronous precursor selection (SPS) was enabled to include 10 MS/MS fragment ions in the FTMS3 scan.

Mass spectrometry data analysis was performed similarly as described above, but TMT modification on the peptide N-termini or lysine residues were enabled for the 16-plex TMT reagents, and deamidation of asparagine and glutamine was included as variable modification in MaxQuant. TPP data analysis was performed using the TPP packages (https://www.bioconductor.org/packages/release/bioc/html/TPP.html) in the R statistical programming language. The data were normalized as detailed in Miettinen et al.[5] (**Supplementary Table 3**).

Data availability

The mass spectrometry proteomics data have been deposited to the ProteomeXchange Consortium[6] via the PRIDE partner repository[7] with the data set identifier: PXD025020. Reviewer account details: Username: reviewer_pxd025020@ebi.ac.uk Password: H0T2rCOL

References

1 Chen, X. *et al.* Ratiometric Mass Spectrometry for Cell Identification and Quantitation Using Intracellular "Dual-Biomarkers". *Sci Rep* **7**, 17432, doi:10.1038/s41598-017-17812-1 (2017).
2 Cox, J. & Mann, M. MaxQuant enables high peptide identification rates, individualized p.p.b.-range mass accuracies and proteome-wide protein quantification. *Nat Biotechnol* **26**, 1367-1372, doi:10.1038/nbt.1511 (2008).
3 Tyanova, S. *et al.* The Perseus computational platform for comprehensive analysis of (prote)omics data. *Nat Methods* **13**, 731-740, doi:10.1038/nmeth.3901 (2016).
4 Huang da, W., Sherman, B. T. & Lempicki, R. A. Systematic and integrative analysis of large gene lists using DAVID bioinformatics resources. *Nat Protoc* **4**, 44-57, doi:10.1038/nprot.2008.211 (2009).
5 Miettinen, T. P. *et al.* Thermal proteome profiling of breast cancer cells reveals proteasomal activation by CDK4/6 inhibitor palbociclib. *EMBO J* **37**, doi:10.15252/embj.201798359 (2018).
6 Deutsch, E. W. *et al.* The ProteomeXchange consortium in 2017: supporting the cultural change in proteomics public data deposition. *Nucleic Acids Res* **45**, D1100-D1106, doi:10.1093/nar/gkw936 (2017).
7 Perez-Riverol, Y. *et al.* The PRIDE database and related tools and resources in 2019: improving support for quantification data. *Nucleic Acids Res* **47**, D442-D450, doi:10.1093/nar/gky1106 (2019).